







# Dual Fabry-Perot interferometers gas pressure sensor in a parallel configuration based on a hollow core Bragg fiber and the harmonic Vernier effect

ZONGRU YANG,<sup>1</sup>  WEIHAO YUAN,<sup>1,\*</sup>  ZHENGANG LIAN,<sup>2</sup>  AND CHANGYUAN YU<sup>1</sup> 

<sup>1</sup>Photonics Research Institute, Department of Electronic and Information Engineering, The Hong Kong Polytechnic University, Hong Kong, China

<sup>2</sup>Yangtze Optical Electronics Co., Ltd. (YOEC), Fifth Hi-Tech Avenue, East Lake Hi-Tech Developzone, Wuhan 430205, China

\*weihao.yuan@connect.polyu.hk

**Abstract:** An ultra-high sensitivity parallel-connected Fabry-Perot interferometers (FPIs) pressure sensor is proposed and demonstrated based on hollow core Bragg fiber (HCBF) and harmonic Vernier effect. The HCBF functions as a micro Fabry-Perot cavity and possesses low transmission loss. One FPI acts as the sensing unit while the other FPI is used as the reference unit to generate the Vernier effect. The sensing FPI was prepared by fusion splicing a section of HCBF between a single-mode fiber (SMF) and a hollow silica tube (HST), and the reference FPI was fabricated by sandwiching a piece of HCBF between two SMFs. Two FPIs with very different free spectral ranges (FSRs) in the fringe pattern were connected to the  $2 \times 2$  coupler parallelly, which realizes the harmonic Vernier effect and ensures the stability of the interference fringe. Laboratory results exhibited that the pressure sensitivity can be enhanced to 119.3 nm/MPa within 0-0.5 MPa by the proposed sensor. Moreover, low-temperature crosstalk of 0.074 kPa/ $^{\circ}$  was achieved. Compared with the traditional optical fiber gas pressure sensor, the advanced sensor features high sensitivity, stability, easy fabrication, and fast response, which can be a promising candidate for real-time and high-precision gas pressure monitoring.

© 2022 Optica Publishing Group under the terms of the [Optica Open Access Publishing Agreement](#)

## 1. Introduction

Optical fiber gas pressure sensors have been widely used in various sensing areas such as environmental safety monitoring, aerospace, military, and medical diagnosis due to their compact size, high accuracy, corrosion resistance, remote monitoring ability, and immunity to electromagnetic interference. Several kinds of structures for gas pressure measurement have been developed based on long-period fiber gratings (LPFGs) [1], fiber Bragg gratings (FBGs) [2], anti-resonant reflecting optical waveguides (ARROWs) [3], Mach-Zehnder interferometers (MZIs) [4], and Fabry-Perot interferometers (FPIs) [5]. Among them, considering robustness and convenient manufacturing, FPIs have been extensively employed recently [6] to estimate the gas pressure via observing changes in the refractive index (RI) or cavity length of the FPI. The structure of fiber optic FPI gas pressure sensors can be divided into two categories: (i) diaphragm-based FPIs, where the light propagates in the closed cavity formed by the diaphragm and fiber end face, and (ii) open FPIs that contain a gas inlet channel connecting from the outside environment to FPI.

For diaphragm-based FPIs, a variety of materials have been employed, including polymer [7], graphene [8], silver [9], and silica [10], which are typically assembled at the end of the sensor and function as the reflector of FPI. The elastic deformation of the diaphragm material induced by pressure variation would further result in the change of optical length of the Fabry-Perot (FP)

cavity. Diaphragm-based FPIs have been reported an ultra-high sensitivity up to  $1.41 \mu\text{m/kPa}$  [7], which rests with the characteristics and shape of the diaphragm. However, these kinds of sensors are generally limited by poor mechanical strength and narrow measuring range since the diaphragm fixed at the fiber end can be easily cracked. Furthermore, the unpredictable mechanical deformation of diaphragm materials could lead to inferior linearity and repeatability.

Open FPIs take advantage of the gas circulating between the intrinsic FP cavity and the external environment. This means the RI of gas in the air cavity will equally change with that outside the cavity, and therefore the linearity and wide sensing range can be guaranteed. There are primary two methods to develop open FPIs. One approach is based on the femtosecond laser drilling technique to create a micro-channel in the side of the fiber [11]. By using this method, this type of sensor possesses high endurance and well fringe visibility. Nonetheless, the fabrication devices are generally pricey and complex, and the debris produced from laser drilling usually disturbs the quality of the interference pattern. Another scheme can be realized by cascading a hollow silica tube (HST) to the FPI without any non-fiber optic assemblies, which indicates its durability and fast response. The air hole of HST could serve as a gas channel while the facet of HST functions as a reflector of FPI. Due to the easy operation, flexible combination, and low cost, this structure is certainly competitive in gas pressure measurement. However, a theoretical analysis proves that the sensitivity of open FPI gas sensors is limited below  $5 \text{ nm/MPa}$  [12], which restricts their practical application expecting high sensitivity. Accordingly, maintaining a large measuring range while ensuring relatively high sensitivity is the major motivation for optical fiber gas pressure sensing.

To improve the sensitivity of open structure gas pressure sensors, FPI sensors based on the Vernier effect have been extensively studied [13–15]. Similar to the Vernier caliper, the optical Vernier effect refers to a reference interferometer as a fixed scale and a sensing interferometer as a sliding part, and the overlap between two interference signals with a slight free spectral range (FSR) difference would generate a superimposed spectrum. The combined spectrum with a periodic envelope can provide a wavelength shift magnification. By detecting the response of the extracted spectrum envelope, the sensing capabilities can be amplified by an order of magnitude compared to that of the individual sensing interferometer, leading to a new generation of high-resolution fiber optic devices. Nowadays, research based on the optical Vernier effect has been proposed for analyzation of a diverse range of parameters, such as curvature [16], temperature [17], strain [18], refractive index [19], and gas pressure [20]. For gas pressure sensing, in 2015, Quan et al. [21] proposed a cascaded-cavity FPI gas pressure sensor using the PCF and the hollow silica tube (HST), which realized a gas pressure sensitivity as high as  $82 \text{ nm/MPa}$ . In 2019, Li et al. [22] arranged single-mode fiber (SMF), side-opened HST, and optical fiber column in series, whose gas pressure sensitivity reached  $80.3 \text{ nm/MPa}$ . In fact, since two FPIs in the cascaded configuration are located physically close to each other, this can probably lead to the unsteadiness of reference signals caused by the change in measurands, which can further influence the accuracy of output signals. Additionally, their temperature cross-sensitivity cannot be ignored as the HST is less sensitive to temperature than the PCF/SMF.

In this paper, we introduced harmonics to the optical Vernier effect and proposed an ultra-high sensitivity fiber gas pressure sensor with two separated FPIs. The harmonic Vernier effect is an extended concept of the fundamental Vernier effect [23]. Theoretically, the fundamental case occurs when the difference between the two optical path lengths (OPLs) is tiny, while the harmonic Vernier effect is that the OPL of the reference unit pluses multiple integers ( $i, i \geq 0, i$  being the harmonic order) of the OPL of the sensing unit. Compared to the fundamental Vernier effect, the harmonic case has further promoted the sensing ability, where the magnification factor is in proportion to the harmonic order. For the proposed sensor, these FPIs are based on the SMF-HCBF-HST (open FPI) structure, and the SMF-HCBF-SMF (closed FPI) structure, respectively. As an air cavity of FPI, the HCBF has the advantage of low transmission loss

that allows the cavity length to be extended to the millimeter-scale, which improves the sensing performance. An inner diameter of the HST much smaller than that of the HCBF provides the mirror reflection and the gas channel. The open FPI as the sensing element and the closed FPI as the reference part are both connected by a 3-dB coupler in a parallel configuration. Two FPIs with very different OPLs generate the first-order ( $i = 1$ ) optical harmonic Vernier effect. In the experiment, the proposed sensor demonstrated a tremendous gas pressure sensitivity of 119.3 nm/MPa ranging from 0 MPa to 0.5 MPa with high linearity of 0.9974, which is 29.24 times larger than the individual sensing interferometer. Moreover, a fairly low-temperature crosstalk of 0.074 kPa/° was realized benefiting from the low thermo-optical coefficient and thermal expansion coefficient of the FP cavity.

## 2. Fabrication and principle

### 2.1. Sensor fabrication

Figure 1 (a) and (b) illustrates the schematic diagram of the proposed gas pressure sensor, which is constructed by two FPIs in a parallel configuration. The commercial fusion splicer (FURUKAWA, FITELE S178A) was used for splicing. To ensure the ideal mechanical strength of the splicing joint and non-deformation of the air core, fusion splicing parameters were optimized, as indicated in Table 1. The sensing unit denoted as FPI-1 was fabricated by fusion splicing a section of the homemade HCBF between the SMF (Corning, SMF28) and the HST (Polymicro Technologies, TSP005150), as shown in Fig. 1(a). The gas diffuses from the ambient environment to the air cavity of HCBF through the hollow core of HST, in the meanwhile, the head face of HST serves as a reflector. There is an offset between the size of the gas inlet channel and the reflection ratio, hence an HST inner/outer diameter of 5/125  $\mu\text{m}$  was chosen to ensure sufficient mirror reflection and fast response. It is noted that the last end face of HST must be polished to avoid redundant reflection. As depicted in Fig. 1(b), the reference unit named FPI-2 was formed by sandwiching a piece of HCBF between two SMFs. The gas tightness of the FPI-2 and isolation of two interferometers guarantee that the referenced interference pattern can avert being disturbed by the outside environment. When light propagates from the lead-in SMF to the air cavity of HCBF, multiple reflections happen at two interfaces M1 and M2. Then both FPI-1 and FPI-2 generate periodic comb-like fine reflection spectra.

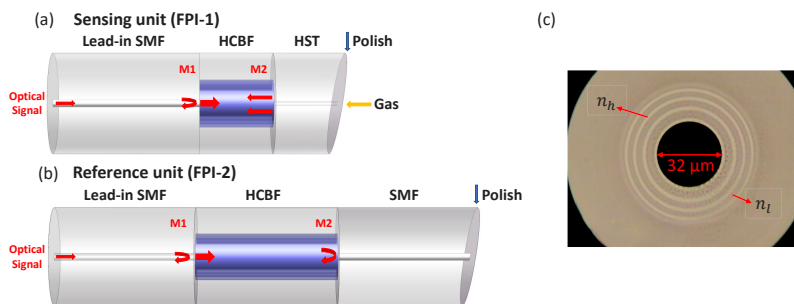


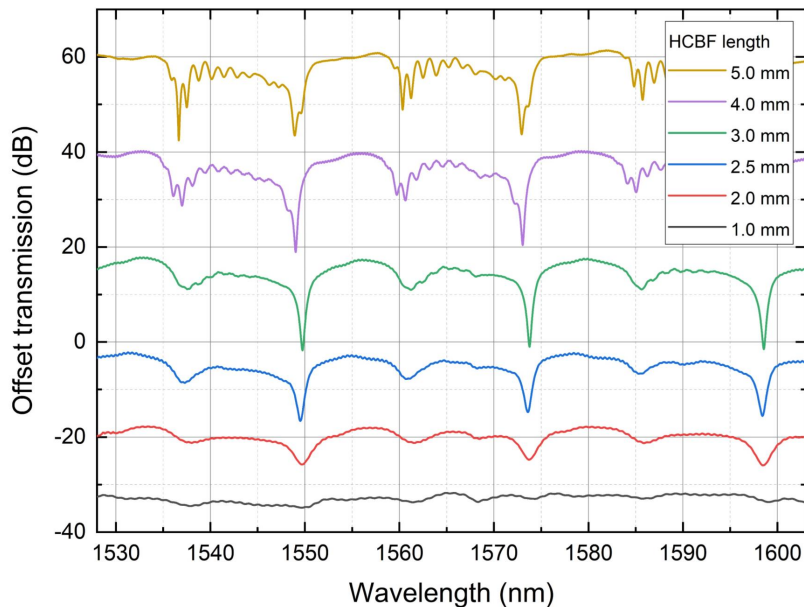
**Fig. 1.** Schematic diagram of the HCBF-based parallel-connected FPIs gas pressure sensor: (a) sensing unit; (b) reference unit. (c) Microscope image of the cross-section of the HCBF.

The microscope image of the cross-section of homemade HCBF is presented in Fig. 1(c). The HCBF has a core/cladding diameter of 32/125  $\mu\text{m}$  and a four-bilayers annular rings structure surrounding the air core. The four pairs of bilayers structure have alternant high and low RIs distribution ( $n_h$  and  $n_l$ , respectively), which can strongly confine light in the air core. Unlike the HST, which is usually used as the air cavity of the FPI [24], the homemade HCBF based on the ARROW mechanism [25] has a comparatively low transmission loss that can offer a well-defined

**Table 1. Main parameters of fusion splicing**

Splicing Parameter	Value
Arc power	60 unit
Arc duration	230 ms
Cleaning offset	60 unit
Cleaning duration	20 ms
Gap	5 $\mu\text{m}$
Z push length	15 $\mu\text{m}$
Arc offset	-10 $\mu\text{m}$

interference as a result [26]. The detailed parameters and fabrication process can be referred to Ref. [27]. To investigate the property of the HCBF, six HCBFs are prepared with different lengths, and their transmission spectra are demonstrated in Fig. 2. Several sharp transmission lossy dips occur at certain resonant wavelengths caused by anti-resonant reflecting [28] when the fiber length is larger than 2.5 mm, which may affect the modulation of the superposition spectrum envelope. Therefore, HCBF lengths of about 1mm and 2 mm with modest profiles in transmission were selected for manufacturing the sensing unit and reference unit, respectively.

**Fig. 2.** Transmission spectra of HCBFs with different lengths.

## 2.2. Fundamental Vernier effect

For a single interferometer, the center wavelength of the  $m$  order ( $m$  being an integer beginning from 1) interference dip in the reflection spectrum can be defined as:

$$\lambda_m = \frac{4nL}{2m+1} = \frac{4}{2m+1} OPL, \quad (1)$$

where  $n$  and  $L$  denote the RI and the cavity length of FPI, respectively. And  $OPL = nl$  is the optical path length, which is an important quantity of the interferometer that determines the FSR.

The FSR of two FPIs can be expressed as:

$$FSR_1 = \frac{\lambda^2}{2n_1L_1}, FSR_2 = \frac{\lambda^2}{2n_2L_2}, \quad (2)$$

where  $FSR_1$  and  $FSR_2$  are the FSR of the sensing unit and reference unit, respectively. Both FPIs are parallel-connected by a 3-dB coupler, which allows the reference unit to be independent of the sensing unit and to maintain stability. Two reflection beams from each FPI recombine as an overlapped spectrum at the coupler and output to the detection system. When OPLs of two interferometers exist a tiny detuning ( $\delta = OPL_1 - OPL_2$ ), the Vernier effect is generated, and the superposition spectrum is modulated by a periodic envelope with fine fringes. The FSR of the envelope can be expressed by the relationship between the FSRs of each interferometer [29]:

$$FSR_e = \left| \frac{FSR_1 \cdot FSR_2}{FSR_1 - FSR_2} \right| = \left| \frac{\lambda^2}{2(n_1L_1 - n_2L_2)} \right|. \quad (3)$$

Since the fringes of the sensing element move slightly, there will be a significant wavelength shift in the Vernier-like spectrum envelope, which amplifies the sensitivity of a single sensing interferometer dozens of times. Therefore, a magnification factor ( $M$  factor) is performed to define the ratio between FSRs of the Vernier envelope and the single sensing probe, such as:

$$M = \frac{FSR_e}{FSR_1} = \left| \frac{FSR_2}{FSR_1 - FSR_2} \right| = \left| \frac{n_1L_1}{n_1L_1 - n_2L_2} \right|. \quad (4)$$

Alternatively, the  $M$  factor can also be defined as the comparison of sensitivity between the Vernier-based sensor and the individual sensing FPI:

$$M = \frac{S_e}{S_1}, \quad (5)$$

where  $S_e$  and  $S_1$  represent the sensitivity of the combined spectrum envelope and the individual sensing unit, respectively. Basically, both definitions of the  $M$  factor can estimate approximately the same result, though their formulas are distinct.

### 2.3. Harmonic Vernier effect

The essential condition of the fundamental Vernier effect is that OPLs of both FPIs should be similar but not equal, nevertheless, the application of the harmonic Vernier effect provides the possibility to fabricate two interferometers with great distinction in the OPL. Harmonics of the Vernier effect relies on the OPL of reference FPI being increased by  $i$  ( $i \geq 0$ ,  $i$  being an integer) multiples of the OPL of sensing FPI ( $OPL_2^i = n_2L_2 + in_1L_1$ ), where  $i$  is the harmonic order. According to Eq. (2), the FSR of the reference FPI becomes:

$$FSR_2 = \frac{\lambda^2}{2(n_2L_2 + in_1L_1)}. \quad (6)$$

It is worth noting that the case  $i = 0$  signifies the fundamental Vernier effect. The harmonics introduced re-forms the envelope intensity with the same frequency and FSR, which can be

verified by the FSR formula of harmonic Vernier-based spectrum as follows [23]:

$$FSR_e^i = \left| \frac{FSR_1 \cdot FSR_2^i}{FSR_1 - (i+1)FSR_2^i} \right| = \left| \frac{\lambda^2}{2(n_1L_1 - n_2L_2)} \right| = FSR_e. \quad (7)$$

The  $M$  factor depends on the concept of the internal envelope [23], which is related to the order of harmonics. In consequence, the  $M$  factor as a function of  $i$  is defined as:

$$M^i = \left| \frac{(i+1)FSR_2^i}{FSR_1 - (i+1)FSR_2^i} \right| = (i+1) \left| \frac{n_1L_1}{n_1L_1 - n_2L_2} \right| = (i+1)M. \quad (8)$$

From Eqs. (7) and (8), it is apparent that the sensitivity can be increased by  $i$  times with the same FSR of envelope via leading in harmonics. Furthermore, Eq. (8) can be modified in the form related to the OPL of the sensing FPI and detuning as:

$$M^i = (i+1) \frac{OPL_1}{\delta}, \quad (9)$$

where a positive or negative detuning factor determines the wavelength shift of envelope peaks is in the forward or opposite direction to that of the individual sensing FPI.

#### 2.4. Sensing mechanism

For gas pressure sensing, the crucial parameter of the proposed structure is the OPL of the cavity, which means that changes in both RI ( $n$ ) and cavity length ( $L$ ) could induce wavelength shift. It should be noted that the change of cavity length of the in-line open cavity FPI directedly induced by pressure is negligible. Thus, the sensitivity is primarily contributed by variation of the RI as a result. According to the updated Edlen equation [30],  $n$  is the function of the temperature and the pressure:

$$n_{air} = 1 + \frac{2.8793 \times 10^{-9}}{1 + 0.00367 \times T} \cdot P, \quad (10)$$

where  $T$  stands for temperature in degrees Celsius ( $^{\circ}$ ), and  $P$  denotes the gas pressure in Pascal (Pa). Therefore, the pressure sensitivity of the sensing FPI can be simply derived from Eq. (1) and Eq. (10) as:

$$\begin{aligned} S_P &= \frac{\partial \lambda_1}{\partial P} \\ &= \frac{4L_1}{2m+1} \cdot \frac{\partial n_{air}}{\partial P} \\ &= \lambda_1 \frac{\partial n_{air}}{\partial P} \cdot \frac{1}{n_{air}} \\ &= \lambda_1 \frac{2.8793 \times 10^{-9}}{1 + 0.00367 \times T} \cdot \frac{1}{n_{air}}. \end{aligned} \quad (11)$$

Typically, the sensitivity of the sensing FPI at a temperature of  $25^{\circ}$  and wavelength of 1550 nm is 4.09 nm/MPa according to Eq. (11), which indicates the pressure sensitivity of the in-line FPI is nearly constant and is irrelevant to the cavity length. Since the variation of temperature has little influence on the RI of air, the sensitivity of temperature is mainly from the thermal expansion effect induced cavity length change:

$$S_T = \frac{\partial \lambda_1}{\partial T} = \lambda_1 \frac{\partial L_1}{\partial T} \cdot \frac{1}{L_1}, \quad (12)$$

where  $(\partial \lambda_1 / \partial T) \cdot (1/L_1)$  is the thermal expansion coefficient of the silica. For the proposed sensor in parallel configuration based on the first-order harmonic Vernier effect, the pressure



sensitivity can be obtained by multiple Eq. (8) and Eq. (11):

$$S_p^1 = M^1 S_p, \quad (13)$$

where  $M^1$  is the magnification factor for the first-order harmonics of the Vernier effect.

### 3. Experimental result and discussion

#### 3.1. Gas pressure experiment

Both FPIs of the proposed sensor have the same RI of the air cavity ( $n_1 = n_2 \approx 1$ ). The sensing unit was fabricated with a cavity length of  $\sim 0.96$  mm, and the cavity length of the reference unit was cleaved to  $\sim 1.85$  mm ( $0.96\text{mm} \times 2$  minus a detuning of  $\sim 70$   $\mu\text{m}$ ) for the production of first-order harmonics. To investigate the properties of each FPI and the harmonic Vernier effect, reflection spectra of the sensing unit, reference unit, and the proposed sensor were analyzed, as shown in Fig. 3. The maximum reflection intensity of the superposition spectrum occurs when the interference peaks of the two FPIs are in phase (black dash line) as depicted in Fig. 3(a), and the space between the two peaks is measured to be 17.42 nm. Moreover, the range between two maximum interference peaks are corresponding to the FSR of the upper envelope (blue curve) of the combined spectrum and the measured FSR is 17.59 nm, as presented in Fig. 3(b). Similarly, the lower envelope (red curve) with the FSR of 17.77 nm is nearly equal to the upper one. The little difference among the three FSRs comes from errors in the envelope fitting process.

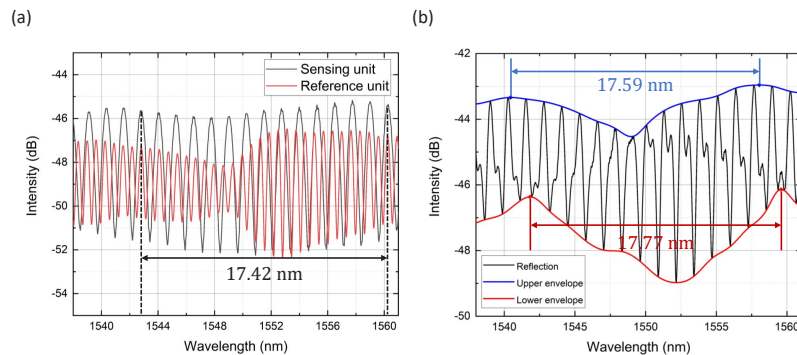


**Fig. 3.** (a) Reflection spectra of the sensing unit and reference unit. (b) Reflection spectrum of the paralleled FPIs.

The Fast Fourier Transform (FFT) was executed to verify the interference reflection of each unit. Figure 4 demonstrates the harmonic Vernier spectral characteristics around the wavelength of 1550 nm, where two dominant peaks located at frequencies of  $0.7996 \text{ nm}^{-1}$  and  $1.5435 \text{ nm}^{-1}$  can be observed, implying that two interferences are generated. According to Eq. (2) and the formula  $FSR = 1/f$  ( $f$  being the frequency), we can conclude that peaks at  $0.7996 \text{ nm}^{-1}$  ( $FSR_1 = 1.2506 \text{ nm}$ ) and  $1.5435 \text{ nm}^{-1}$  ( $FSR_2 = 0.6479 \text{ nm}$ ) are frequencies of the sensing unit and the reference unit, respectively. The minor peak at the frequency of  $2.3488 \text{ nm}^{-1}$  represents the partial reflection between the two interfaces of the HST. As the detuning is positive, the redshift would happen when pressure is increased. And the theoretical FSR of the envelope is calculated to be 17.95 nm, which is in line with the experimental result. In this context, the M factor is estimated to be 28.71 according to Eq. (8).

The schematic diagram of the experimental setup for gas pressure sensing based on the harmonic Vernier effect and the HCBF is displayed in Fig. 5. Both the sensing unit and reference unit were parallelly connected to the output arms of the 3-dB coupler. The incident light launching

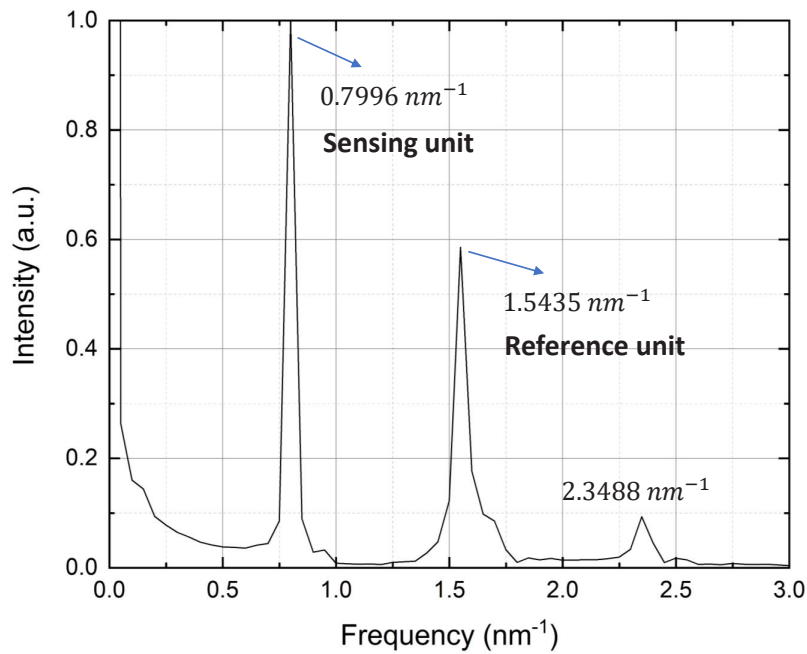


Fig. 4. FFT for the superimposed interference spectrum.

from the amplified spontaneous emission (ASE; MC Fiber Optics) with a spectral range of 1528–1603 nm was guided into the coupler and was divided equally into two parts. One part propagated to the sensing unit while another one was transmitted to the reference unit. Then the reflection beams overlapped at the coupler and were detected by the optical spectrum analyzer (OSA; Yokogawa, AQ6374) with a resolution of 0.05 nm. The sensing unit was sealed into the chamber of the pressure test bench (MY Instrument Technology Co., Ltd., YFY-XK600) using ultraviolet (UV) glue. A high-accuracy pressure gauge (MY Instrument Technology Co., LTD., GJ100-M05) was installed on the bench to measure the pressure with a precision of 0.0001 MPa.

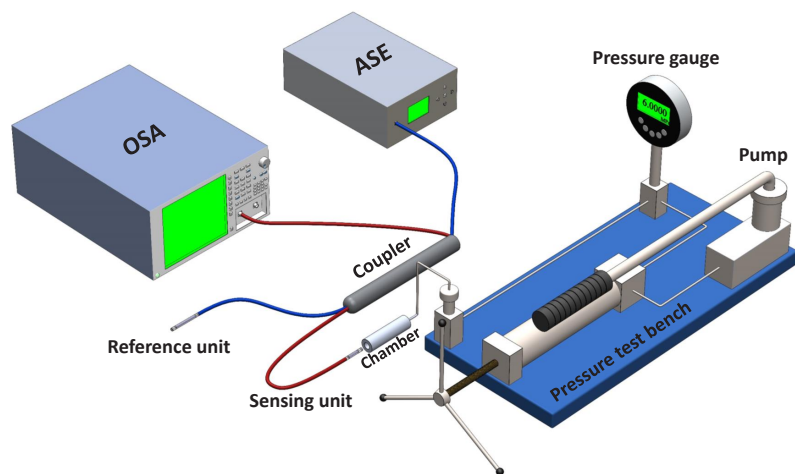
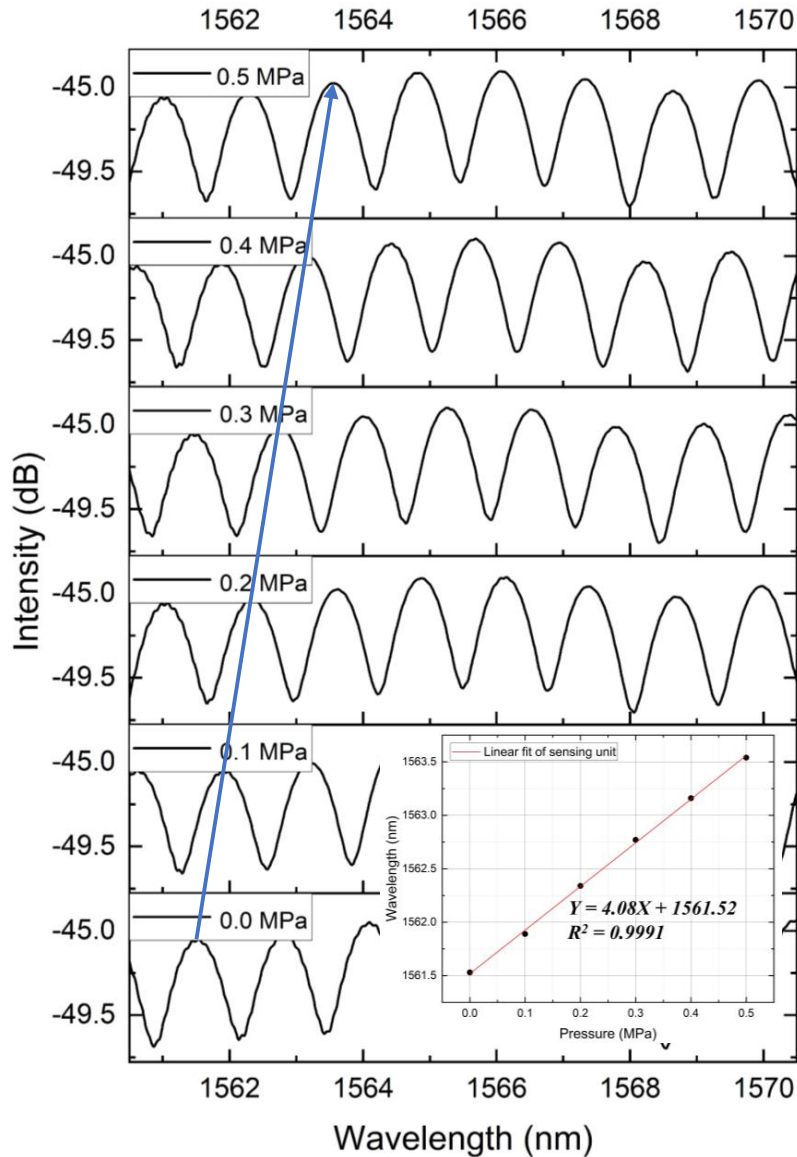


Fig. 5. Schematic diagram of the experimental setup for gas pressure measurement.



To verify the magnification of the proposed sensor compared to a single sensing part, the pressure measurement was firstly conducted for the sensor without the reference unit. In Fig. 6, the interference peak situates at the wavelength of around 1560.9 nm discloses a wavelength shift toward the longer wavelength as the pressure increases in the interval of 0-0.5MPa with a step of 0.1 MPa. The inset shows that the sensitivity of the sensing FPI for pressure increasing is measured to be 4.08 nm/MPa, which is identified with the theoretical result of Eq. (11).



**Fig. 6.** Response of the sensing FPI to pressure, inset shows the relationship between the wavelength of interference peak and pressure.

For the paralleled structure sensor, gas pressure experiments were repeated with pressure increasing and decreasing from 0 MPa to 0.5 MPa with a step of 0.02 MPa at room temperature

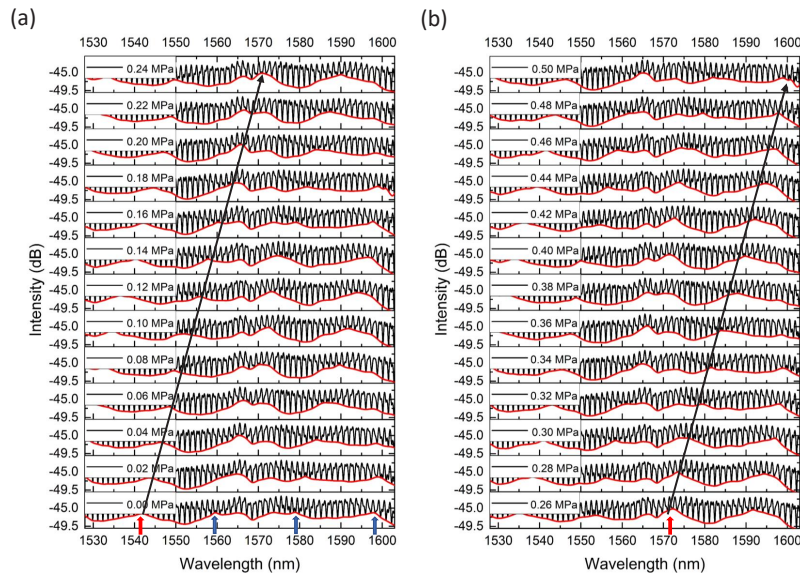


**Fig. 7.** Response of the paralleled FPIs to pressure: (a) pressure ranges from 0.00 MPa to 0.24 MPa; (b) pressure ranges from 0.26 MPa to 0.50 MPa.

( $\sim 23.5^\circ$ ). Reflection spectra under multiple pressure values within 0.00–0.24 MPa and 0.26–0.50 MPa are shown in Fig. 7(a) and Fig. 7(b), respectively. The lower envelope (red line) of the reflection spectrum with a distinct outline is selected for analysis. Four envelope peaks (red and blue arrows) in the range from 1528 nm to 1603 nm can be detected in Fig. 7(a). The peak pointed by the red arrow at the wavelength of about 1542 nm was arranged to be the traced peak, beginning from the gas pressure of 0 MPa. As pressure rises, the envelope peak reveals a steady and remarkable redshift indicated by black straight arrows, which is consistent with the theory. As shown in Fig. 8, the pressure sensitivity in the process of pressure increase is measured to be 119.29 nm/MPa, with the R-squared value of 0.9973. Inversely, the blueshift of the Vernier envelope occurs when the pressure reduces, and the calculated slope is 119.26 nm/MPa with a linearity of 0.9974. The experimental results in both processes of pressures increasing and decreasing demonstrate excellent sensing performance of the proposed sensor, which has ultra-high sensitivity and great linearity, and the similarity of results from the two groups signifies the high repeatability. An  $M$  factor of 29.24 is obtained according to Eq. (13), and it is similar to the estimated value.

### 3.2. Temperature experiment

The HCBF-based harmonic Vernier sensor was placed in a temperature chamber, and the value of temperature was adjusted from 25 °C to 55 °C with a step of 10 °C. Figure 9 shows the reflection spectra of a single envelope under different temperatures, which specify the blueshift trend of the envelope peak with temperature increasing. It can be distinctly observed that the peak wavelength presents a tiny shift in a large temperature range. The inset from Fig. 9 exhibits the linear response of the peak wavelength to the change in temperature, and the fitting slope is calculated to be  $-8.8 \text{ pm}/^\circ\text{C}$  with a linearity of 0.9954. Compared to the wavelength shift of the envelope peak caused by pressure change, that induced by temperature is negligible. The temperature crosstalk is calculated to be about  $0.074 \text{ kPa}/^\circ$ , which means that the proposed HCBF-based sensor can realize temperature-insensitive pressure sensing.

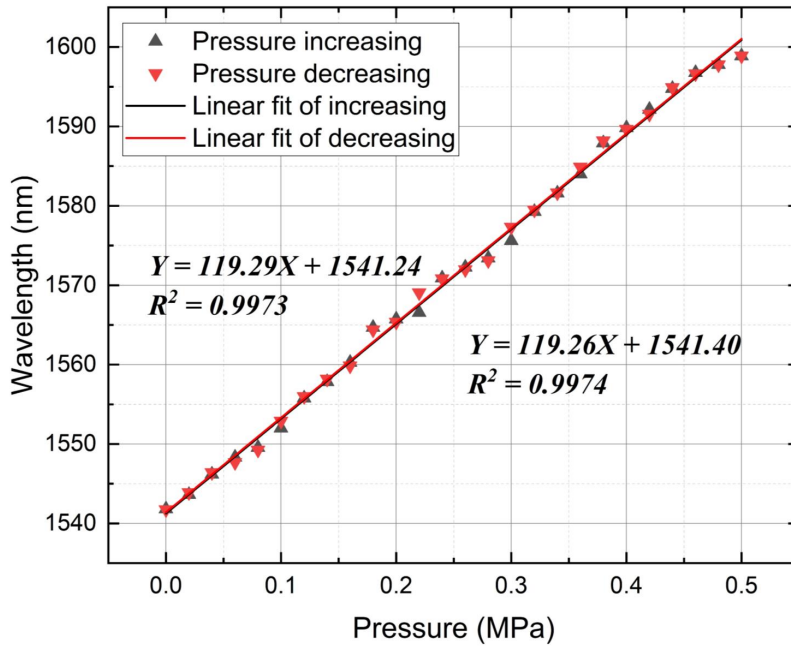


**Fig. 8.** Relationship between the wavelength of envelope peak and pressure with pressure increasing and decreasing.

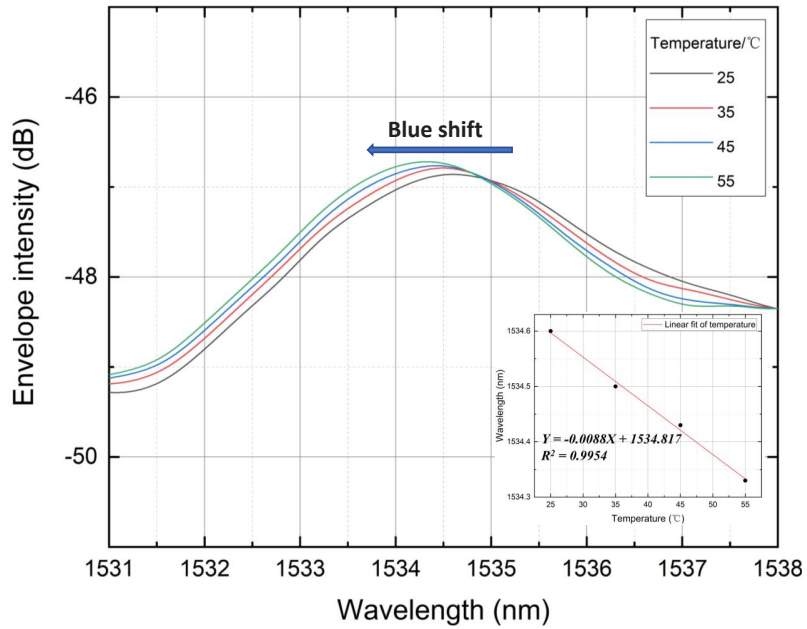


**Fig. 9.** Response of the paralleled FPIs to temperature, inset shows the relationship between the wavelength of envelope peak and temperature.

### 3.3. Discussion

Practically, the length of in-line FPIs based on the fundamental Vernier effect is commonly at a sub-millimeter scale to reduce the transmission loss for a relatively high extinction ratio of the reflection spectrum. By using the HCBF, the cavity length can be extended to the millimeter-scale benefiting from its low transmission loss [31], which can significantly simplify the fabrication process. In addition, since the  $M$  factor is inversely proportional to the detuning, it can be challenging to maintain small detuning for high sensitivity at the cavity length of the sub-millimeter scale by manual slicing. But harmonics of the Vernier effect can provide higher sensitivity, meaning that harmonics allow for higher interferometer fabrication tolerances. Besides, the  $M$  factor is proportional to the OPL of the sensing unit, the millimeter-scale OPL can contribute to the magnification. It is noted that the large FSR of the envelope induced by the short cavity length or tiny detuning will limit the detection system with narrow bandwidth.

When the  $M$  factor increases with the harmonic order beyond limitation, there is a trade-off between the sensitivity and the visibility of the reflection spectrum envelope as the increasing harmonic order will result in the evanescence of envelope peaks [23]. Since the increase of harmonic order corresponds to the increase of HCBF length for the proposed sensor, the second harmonic order (length  $\sim 3$  mm) can damage the envelope profiles due to the anti-resonant reflecting.

The comparisons of key sensing parameters between the proposed sensor and other reported gas pressure sensors with diverse structures based on the Vernier effect are shown in Table 2. Among them, the pressure sensitivity of the proposed sensor in this work is far ahead. Both high detunings of the sensor reported in this work and Ref. [24] based on the first-order harmonics present great sensitivity with a relatively high detuning factor, which verifies the high fabrication tolerance of the harmonic Vernier effect-based sensor. With parallel configuration, sensors reported in this work and Ref. [32] have the characteristic of low-temperature crosstalk. Additionally, the pressure sensing range can be enlarged while the light source with broader bandwidth is used.

**Table 2. Performances of gas pressure sensors based on the Vernier effect**

Structure	Sensitivity (nm/MPa)	$M$ factor	$\delta$ ( $\mu\text{m}$ )	Pressure sensing range (MPa)	Temperature crosstalk (kPa/ $^{\circ}$ )	Ref.
FPI: HCBF + HST and HCBF + SMF in parallel	119.29	29.24	$\sim 70$	0-0.5	0.074	This work
FPI: HST + PCF in series	-82	26.36	-8.1	0-1.379	-	[21]
FPI: SMFs in side-opened HST	-86.64	32.8	-21.9	0-0.6	5.18	[20]
FPI: side-opened HST + SMF in series	80.3	$\sim 20$	18.1	0.1-0.3	-1.33	[22]
FPI: HSTs in series (first-order harmonics)	80.8	-	40	0.001-0.1	2.22	[24]
FPI: cascaded HSTs and HST + SMF in parallel	45.76	11.44	11	0-1.2	0.097	[32]
MZI: MMF + dual side hole fiber + MMF in series	-60	$\sim 7$	23	0-0.8	0.55	[33]
MZI: MMF + HST + MMF + side-opened HST+ MMF in series	-73.32	8.5	-	0-0.8	0.72	[4]

#### 4. Conclusion

In summary, a harmonic Vernier effect-based parallel-connected FPI sensor using HCBF is proposed and demonstrated for pressure measurement. First-order harmonics introduced in the Vernier effect can further magnify the sensitivity and enhance the fabrication tolerance. With the unique structure, the HCBF facilitates light confinement, providing the possibility of elongating the cavity length, which can boost the magnification factor of the proposed sensor. The use of HCBF and harmonic Vernier effect makes it possible to obtain a high sensitivity without the need to focus on reducing OPL differences, which simplifies the fabrication process. According to the response of the lower envelope peak, the measured pressure sensitivity of the proposed sensor is 119.29 nm/MPa in the range of 0-0.5 MPa, with linearity of 0.9973, and the magnification factor reaches as high as 29.24. The sensitivity of temperature is -8.8 pm/°C ranging from 25 °C to 55 °C, and the corresponding linearity is 0.9954. Extremely low-temperature crosstalk of 0.074 kPa° is achieved. The ultra-high sensitivity, low-temperature crosstalk, compact size, cost-effective production, and simplicity will make the advanced sensor continuously progress in the sensing area.

**Funding.** Shenzhen Municipal Science and Technology Innovation Commission, Shenzhen-HK-Macao Science and Technology Plan C (SGDX2020110309520303).

**Disclosures.** The authors declare no conflicts of interest.

**Data availability.** Data underlying the results presented in this paper are not publicly available at this time but may be obtained from the authors upon reasonable request.

#### References

1. X. Zhong, Y. Wang, C. Liao, S. Liu, J. Tang, and Q. Wang, "Temperature-insensitivity gas pressure sensor based on inflated long period fiber grating inscribed in photonic crystal fiber," *Opt. Lett.* **40**(8), 1791–1794 (2015).
2. Q. Zhang, N. Liu, T. Fink, H. Li, W. Peng, and M. Han, "Fiber-optic pressure sensor based on  $\pi$ -phase-shifted fiber bragg grating on side-hole fiber," *IEEE Photonics Technol. Lett.* **24**(17), 1519–1522 (2012).
3. Y. Wang, J. Tao, W. Yuan, Z. Lian, Q. Ling, D. Chen, Z. Yu, and C. Lu, "Hollow core bragg fiber integrated with regenerate fiber bragg grating for simultaneous high temperature and gas pressure sensing," *J. Lightwave Technol.* **39**(17), 5643–5649 (2021).
4. Y. Zhao, H. Lin, C. Zhou, H. Deng, A. Zhou, and L. Yuan, "Cascaded mach-zehnder interferometers with vernier effect for gas pressure sensing," *IEEE Photonics Technol. Lett.* **31**(8), 591–594 (2019).
5. Z. Zhang, J. He, Q. Dong, Z. Bai, C. Liao, Y. Wang, S. Liu, K. Guo, and Y. Wang, "Diaphragm-free gas-pressure sensor probe based on hollow-core photonic bandgap fiber," *Opt. Lett.* **43**(13), 3017–3020 (2018).
6. Z. Zhang, Y. Wang, M. Zhou, J. He, C. Liao, and Y. Wang, "Recent advance in hollow-core fiber high-temperature and high-pressure sensing technology," *Chin. Opt. Lett.* **19**(7), 070601 (2021).
7. J. Eom, C.-J. Park, B. H. Lee, J.-H. Lee, I.-B. Kwon, and E. Chung, "Fiber optic fabry-perot pressure sensor based on lensed fiber and polymeric diaphragm," *Sens. Actuators, A* **225**, 25–32 (2015).
8. J. Ma, W. Jin, H. L. Ho, and J. Y. Dai, "High-sensitivity fiber-tip pressure sensor with graphene diaphragm," *Opt. Lett.* **37**(13), 2493–2495 (2012).
9. F. Xu, D. Ren, X. Shi, C. Li, W. Lu, L. Lu, L. Lu, and B. Yu, "High-sensitivity fabry-perot interferometric pressure sensor based on a nanothick silver diaphragm," *Opt. Lett.* **37**(2), 133–135 (2012).
10. C. Liao, S. Liu, L. Xu, C. Wang, Y. Wang, Z. Li, Q. Wang, and D. Wang, "Sub-micron silica diaphragm-based fiber-tip fabry-perot interferometer for pressure measurement," *Opt. Lett.* **39**(10), 2827–2830 (2014).
11. M. Hou, F. Zhu, Y. Wang, Y. Wang, C. Liao, S. Liu, and P. Lu, "Antiresonant reflecting guidance mechanism in hollow-core fiber for gas pressure sensing," *Opt. Express* **24**(24), 27890–27898 (2016).
12. G. Z. Xiao, A. Adnet, Z. Zhang, Z. Lu, and C. P. Grover, "Fiber-optic fabry-perot interferometric gas-pressure sensors embedded in pressure fittings," *Microw. Opt. Technol. Lett.* **42**(6), 486–489 (2004).
13. A. D. Gomes, H. Bartelt, and O. Fraz ao, "Optical vernier effect: recent advances and developments," *Laser Photonics Rev.* **15**(7), 2000588 (2021).
14. Y. Liu, X. Li, Y.-N. Zhang, and Y. Zhao, "Fiber-optic sensors based on vernier effect," *Measurement* **167**, 108451 (2021).
15. Y. Chen, L. Zhao, S. Hao, and J. Tang, "Advanced fiber sensors based on the vernier effect," *Sensors* **22**(7), 2694 (2022).
16. S. Zhang, Y. Liu, H. Guo, A. Zhou, and L. Yuan, "Highly sensitive vector curvature sensor based on two juxtaposed fiber michelson interferometers with vernier-like effect," *IEEE Sens. J.* **19**(6), 2148–2154 (2018).
17. L.-Y. Shao, Y. Luo, Z. Zhang, X. Zou, B. Luo, W. Pan, and L. Yan, "Sensitivity-enhanced temperature sensor with cascaded fiber optic sagnac interferometers based on vernier-effect," *Opt. Commun.* **336**, 73–76 (2015).



18. J. Deng and D. Wang, "Ultra-sensitive strain sensor based on femtosecond laser inscribed in-fiber reflection mirrors and vernier effect," *J. Lightwave Technol.* **37**(19), 4935–4939 (2019).
19. J. Li, M. Zhang, M. Wan, C. Lin, S. Huang, C. Liu, Q. He, X. Qiu, and X. Fang, "Ultrasensitive refractive index sensor based on enhanced vernier effect through cascaded fiber core-offset pairs," *Opt. Express* **28**(3), 4145–4155 (2020).
20. P. Chen, Y. Dai, D. Zhang, X. Wen, and M. Yang, "Cascaded-cavity fabry-perot interferometric gas pressure sensor based on vernier effect," *Sensors* **18**(11), 3677 (2018).
21. M. Quan, J. Tian, and Y. Yao, "Ultra-high sensitivity fabry-perot interferometer gas refractive index fiber sensor based on photonic crystal fiber and vernier effect," *Opt. Lett.* **40**(21), 4891–4894 (2015).
22. Z. Li, Y.-X. Zhang, W.-G. Zhang, L.-X. Kong, T.-Y. Yan, P.-C. Geng, and B. Wang, "High-sensitivity gas pressure fabry-perot fiber probe with micro-channel based on vernier effect," *J. Lightwave Technol.* **37**(14), 3444–3451 (2019).
23. A. D. Gomes, M. S. Ferreira, J. Bierlich, J. Kobelke, M. Rothhardt, H. Bartelt, and O. Fraz ao, "Optical harmonic vernier effect: A new tool for high performance interferometric fiber sensors," *Sensors* **19**(24), 5431 (2019).
24. X. Yang, S. Wu, H. Cheng, J. Ma, S. Wang, S. Liu, and P. Lu, "Simplified highly-sensitive gas pressure sensor based on harmonic vernier effect," *Opt. Laser Technol.* **140**, 107007 (2021).
25. P. Yeh, A. Yariv, and E. Marom, "Theory of bragg fiber," *J. Opt. Soc. Am.* **68**(9), 1196–1201 (1978).
26. W. Yuan, L. Li, Y. Wang, Z. Lian, D. Chen, C. Yu, and C. Lu, "Temperature and curvature insensitive all-fiber sensor used for human breath monitoring," *Opt. Express* **29**(17), 26375–26384 (2021).
27. Z. Liu, M.-L. V. Tse, C. Wu, D. Chen, C. Lu, and H.-Y. Tam, "Intermodal coupling of supermodes in a twin-core photonic crystal fiber and its application as a pressure sensor," *Opt. Express* **20**(19), 21749–21757 (2012).
28. Z. Yang, W. Yuan, and C. Yu, "Hollow core bragg fiber-based sensor for simultaneous measurement of curvature and temperature," *Sensors* **21**(23), 7956 (2021).
29. P. Zhang, M. Tang, F. Gao, B. Zhu, S. Fu, J. Ouyang, P. P. Shum, and D. Liu, "Cascaded fiber-optic fabry-perot interferometers with vernier effect for highly sensitive measurement of axial strain and magnetic field," *Opt. Express* **22**(16), 19581–19588 (2014).
30. K. Birch and M. Downs, "An updated edlén equation for the refractive index of air," *Metrologia* **30**(3), 155–162 (1993).
31. Y. Wang, Y. Zhou, X. Wang, D. Chen, Z. Lian, C. Lu, and H.-Y. Tam, "Simultaneous measurement of temperature and strain based on a hollow core bragg fiber," *Opt. Lett.* **45**(22), 6122–6125 (2020).
32. X. Song, L. Hou, X. Wei, H. Su, C. Li, Y. Li, and L. Ran, "High sensitivity fiber gas pressure sensor with two separated fabry-perot interferometers based on the vernier effect," *Photonics* **9**(1), 31 (2022).
33. H. Lin, F. Liu, H. Guo, A. Zhou, and Y. Dai, "Ultra-highly sensitive gas pressure sensor based on dual side-hole fiber interferometers with vernier effect," *Opt. Express* **26**(22), 28763–28772 (2018).